IOPscience iopscience.iop.org

Home Search Collections Journals About Contact us My IOPscience

Analysis of an exact inversion algorithm for spiral cone-beam CT

This content has been downloaded from IOPscience. Please scroll down to see the full text.

2002 Phys. Med. Biol. 47 2583

(http://iopscience.iop.org/0031-9155/47/15/302)

View the table of contents for this issue, or go to the journal homepage for more

Download details:

IP Address: 129.129.158.198
This content was downloaded on 23/09/2014 at 13:40

Please note that terms and conditions apply.

INSTITUTE OF PHYSICS PUBLISHING PHYSICS IN MEDICINE AND BIOLOGY

Phys. Med. Biol. **47** (2002) 2583–2597 PII: S0031-9155(02)37169-0

Analysis of an exact inversion algorithm for spiral cone-beam CT

Alexander Katsevich

Department of Mathematics, University of Central Florida, Orlando, FL 32816-1364, USA

E-mail: akatsevi@pegasus.cc.ucf.edu

Received 12 December 2001
Published 17 July 2002
Online at stacks.iop.org/PMB/47/2583

Abstract

In this paper we continue studying a theoretically exact filtered backprojection inversion formula for cone beam spiral CT proposed earlier by the author. Our results show that if the phantom f is constant along the axial direction, the formula is equivalent to the 2D Radon transform inversion. Also, the inversion formula remains exact as spiral pitch goes to zero and in the limit becomes again the 2D Radon transform inversion formula. Finally, we show that according to the formula the processed cone beam projections should be backprojected using both the inverse distance squared law and the inverse distance law.

1. Introduction

Spiral computed tomography (CT) involves continuous data acquisition throughout the volume of interest by simultaneously moving the patient through the gantry while the x-ray source rotates. In the past decade it became clear that spiral CT can be significantly improved if one uses two-dimensional detector arrays instead of one-dimensional. However, accurate and efficient image reconstruction from the data provided by such scanners is very challenging because until very recently there did not exist a theoretically exact and efficient reconstruction formula. Several approaches for image reconstruction have been proposed. They can be classified into two groups: theoretically exact and approximate. See Turbell and Danielsson (2000) and Grangeat (2001) for recent reviews of available algorithms. Most of exact algorithms are based on computing the Radon transform for a given plane by partitioning the plane in a manner determined by the spiral path of the x-ray source (Tam 1995, 1997, Kudo and Saito 1997, Schaller *et al* 2000). These algorithms use a relationship between the first derivative of the Radon transform and the cone beam transform (see Grangeat (1991), Ramm and Zaslavsky (1992) and Natterer (1994)). Even though exact algorithms are more accurate, they are computationally quite intensive and require keeping considerable amount of cone beam projections in memory. Approximate algorithms are more efficient (see e.g. Kudo *et al* (1998), Noo *et al* (1998), Defrise *et al* (2000), Bruder *et al* (2000),

0031-9155/02/152583+15$30.00 © 2002 IOP Publishing Ltd Printed in the UK

Kachelriess *et al* (2000), Katsevich (2002a) for several most recent techniques), but produce artefacts, which can be significant under unfavourable circumstances.

In Katsevich (2001b, 2002b) the first theoretically exact inversion formula of the filtered backprojection (FBP) type was proposed. The formula can be numerically implemented in two steps. First, one performs shift-invariant filtering of a derivative of the cone beam projections, and, secondly, the result is back-projected in order to form an image. The price to pay for this efficient structure is that the algorithm requires an array wider than the theoretically minimum one. Also, the algorithm is applicable if the radius of support of the patient inside the gantry is not too big.

In Katsevich (2001a) the author proposed an improved inversion formula, which is still theoretically exact and of the FBP type, but with fewer drawbacks. First, there is no longer any restriction on the size of the patient provided that he/she fits inside the gantry. Secondly, the new algorithm requires a much smaller detector array than the old one. Thirdly, the new algorithm is two times faster than the old one. The results of testing the algorithm on the simulated data are reported in Katsevich (2001a) as well.

In this paper we continue studying the improved algorithm. The following three problems are considered:

(i) What happens with the inversion formula if the phantom does not depend on the axial direction x_3?
(ii) What happens with the inversion formula if the pitch of the spiral h goes to zero?
(iii) How can x-dependence of the backprojection step be simplified? In particular, how do the weights of the backprojection step depend on the distance from a focal point to a reconstruction point?

Our results show that if the phantom f is constant along the axial direction, the formula is equivalent to the 2D Radon transform inversion. Also, the inversion formula stays exact as spiral pitch $h \to 0$ and in the limit becomes again the 2D Radon transform inversion formula. Finally, we show that in the proposed algorithm the backprojection step is very simple. The only two weights needed to backproject the processed cone beam projections are $1/|x - y(s)|$ and $1/|x - y(s)|^2$. Here $|x - y(s)|$ denotes the distance from a focal point $y(s)$ to a reconstruction point x.

2. The main inversion formula

First we introduce the necessary notations. Let

$$C := \{y \in \mathbb{R}^3 : y_1 = R\cos(s),\ y_2 = R\sin(s),\ y_3 = s(h/2\pi),\ s \in \mathbb{R}\} \tag{1}$$

where $h > 0$ be a spiral, and U be an open set strictly inside the spiral

$$\overline{U} \subset \left\{x \in \mathbb{R}^3 : x_1^2 + x_2^2 < r^2\right\} \qquad 0 < r < R \tag{2}$$

S^2 is the unit sphere in $\mathbb{R}^3$, and

$$\begin{aligned} &D_f(y, \Theta) := \int_0^\infty f(y + \Theta t)\,\mathrm{d}t \qquad \Theta \in S^2 \\ &\beta(s, x) := \frac{x - y(s)}{|x - y(s)|} \qquad x \in U \qquad y(s) \in C \end{aligned} \tag{3}$$

that is $D_f(y, \beta)$ is the cone beam transform of f. Also, $\dot{y}(s) := \mathrm{d}y/\mathrm{d}s$.

As was shown in Danielsson *et al* (1997) and Defrise *et al* ((2000)), any point strictly inside the spiral belongs to one and only one PI segment. Let $s = s_b(x)$ and $s = s_t(x)$ denote

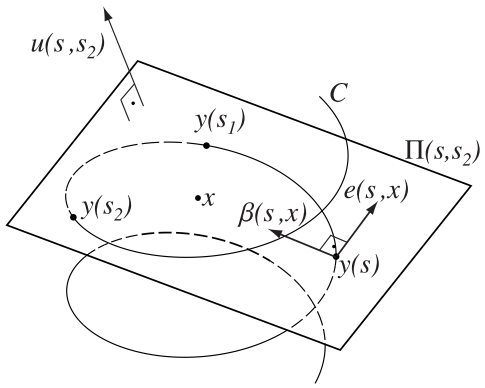

Figure 1. Illustration of the basic construction used in the inversion formula.

values of the parameter corresponding to the endpoints of the PI segment containing x. We will call $I_{PI}(x) := [s_b(x), s_t(x)]$ the PI parametric interval.

Choose any $\psi \in C^\infty([0, 2\pi])$ with the properties

$$\begin{aligned} &\psi(0) = 0 \qquad 0 < \psi'(t) < 1 \qquad t \in [0, 2\pi] \\ &\psi'(0) = 0.5 \qquad \psi^{(2k+1)}(0) = 0 \qquad k \geqslant 1. \end{aligned} \tag{4}$$

Suppose that s, s_1 and s_2 are related by

$$s_1 = \begin{cases} \psi(s_2 - s) + s & s \leqslant s_2 < s + 2\pi \\ \psi(s - s_2) + s_2 & s - 2\pi < s_2 < s. \end{cases} \tag{5}$$

As an example, the function $\psi(t) = t/2$ satisfies conditions (4) and leads to

$$s_1 = (s + s_2)/2 \qquad s - 2\pi < s_2 < s + 2\pi. \tag{6}$$

Denote also

$$\begin{aligned} u(s, s_2) &= \frac{(y(s_1) - y(s)) \times (y(s_2) - y(s))}{|(y(s_1) - y(s)) \times (y(s_2) - y(s))|} \operatorname{sgn}(s_2 - s) \qquad 0 < |s_2 - s| < 2\pi \\ u(s, s_2) &= \frac{\dot y(s) \times \ddot y(s)}{|\dot y(s) \times \ddot y(s)|} \qquad s_2 = s. \end{aligned} \tag{7}$$

It is shown in Katsevich (2001a) that $u(s, s_2)$ is a C^∞ vector function of its arguments. As is easily seen, $u(s, s_2)$ is a unit vector perpendicular to the plane $\Pi(s, s_2)$, which contains $y(s)$, $y(s_1(s, s_2))$, and $y(s_2)$ (see figure 1).

Fix $x \in U$ and $s \in I_{PI}(x)$. Find $s_2 \in I_{PI}(x)$ such that the plane $\Pi(s, s_2)$ contains x (see figure 1). More precisely, we have to solve for s_2 the following equation

$$(x - y(s)) \cdot u(s, s_2) = 0 \qquad s_2 \in I_{PI}(x). \tag{8}$$

It is shown in Katsevich (2001a) that this construction defines a smooth function $s_2 := s_2(s, x)$ and, consequently, $u(s, x) := u(s, s_2(s, x))$. The following inversion formula is proved in Katsevich (2001a).

Theorem 1. *For $f \in C_0^\infty(U)$ one has*

$$f(x) = -\frac{1}{2\pi^2} \int_{I_{PI}(x)} \frac{1}{|x - y(s)|} \int_0^{2\pi} \frac{\partial}{\partial q} D_f(y(q), \Theta(s, x, \gamma))\Big|_{q=s} \frac{\mathrm{d}\gamma}{\sin\gamma}\, \mathrm{d}s \tag{9}$$

where $\Theta(s, x, \gamma) := \cos\gamma\beta(s, x) + \sin\gamma e(s, x)$ and $e(s, x) := \beta(s, x) \times u(s, x)$.

In (9) $\frac{\partial}{\partial q} D_f(y(q), \Theta)$ is the derivative of the cone-beam data with respect to the parameter along the spiral when the direction Θ is fixed. It is shown in Katsevich (2001a) that for a fixed x the integral with respect to γ in (9) reduces to an integral along a tilted line on the detector. By varying x one gets a one-parameter family of tilted lines (see also section 4). The locations and tilts of these lines depend on the function ψ. For the convenience of the reader a sketch of the proof of theorem 1 is presented in appendix A.

3. Two particular cases of the inversion formula

Our first result is the following theorem.

Theorem 2. *Suppose $f(x_1, x_2, x_3) = g(x_1, x_2)$ for some $g \in C_0^\infty$ supported inside the disc $x_1^2 + x_2^2 \leqslant r^2$. Then (9) transforms into the 2D Radon transform inversion formula for g.*

Proof. Let $x \in U$ be fixed. Consider the integral with respect to γ in (9):

$$\begin{aligned} A(s,x) &= \int_0^{2\pi} \frac{\partial}{\partial q} D_f(y(q), \Theta(s,x,\gamma))\Big|_{q=s} \frac{\mathrm{d}\gamma}{\sin\gamma} \\ &= \frac{\partial}{\partial q} \int_0^{2\pi}\int_0^{\infty} f(y(q) + t(\cos\gamma\beta + \sin\gamma e)) \frac{1}{t\sin\gamma} t\,\mathrm{d}t\,\mathrm{d}\gamma\Big|_{q=s} \\ &= \frac{\partial}{\partial q} \int\int_{-\infty}^{\infty} g(y_1(q) + v\beta_1 + we_1, y_2(q) + v\beta_2 + we_2)\,\mathrm{d}v \frac{\mathrm{d}w}{w}\Big|_{q=s} \end{aligned} \tag{10}$$

where

$$v = t\cos\gamma \qquad w = t\sin\gamma \qquad \beta = \beta(s,x) \qquad e = e(s,x)$$

and

$$\beta = (\beta_1, \beta_2, \beta_3) \qquad e = (e_1, e_2, e_3). \qquad \square$$

Denote $\tilde{\beta} = (\beta_1, \beta_2)/\sqrt{\beta_1^2 + \beta_2^2}$, $\tilde{e} = (e_1, e_2)$ (see figure 2). Let $\tilde{e}^\perp$ be the unit vector in the x_1–x_2 plane perpendicular to $\tilde{\beta}$ and defined by $\tilde{e}^\perp = \tilde{\beta} \times j_3$, where j_3 is the unit vector along the x_3 axis. Represent $\tilde{e}$ in the form $\tilde{e} = c_1\tilde{\beta} + c_2\tilde{e}^\perp$. Clearly,

$$c_2 = \tilde{e}\cdot\tilde{e}^\perp = e\cdot\tilde{e}^\perp = (\beta \times u(s,x))\cdot\frac{\beta\times j_3}{\sqrt{\beta_1^2+\beta_2^2}} = \frac{u(s,x)\cdot j_3}{\sqrt{\beta_1^2+\beta_2^2}}. \tag{11}$$

In Katsevich (2001a) it was shown that $u(s,x)\cdot j_3 > 0$. Therefore, $c_2 > 0$. Starting with rescaling v, rewrite (10) as follows:

$$\begin{aligned} A(s,x) &:= \frac{1}{\sqrt{\beta_1^2+\beta_2^2}} \frac{\partial}{\partial q} \int\int_{-\infty}^{\infty} g(\tilde{y}(q) + v\tilde{\beta} + w\tilde{e})\,\mathrm{d}v\frac{\mathrm{d}w}{w}\Big|_{q=s} \\ &= \frac{1}{\sqrt{\beta_1^2+\beta_2^2}} \frac{\partial}{\partial q} \int\int_{-\infty}^{\infty} g(\tilde{y}(q) + (v + c_1 w)\tilde{\beta} + c_2 w\tilde{e}^\perp)\,\mathrm{d}v\frac{\mathrm{d}w}{w}\Big|_{q=s} \\ &= \frac{1}{\sqrt{\beta_1^2+\beta_2^2}} \frac{\partial}{\partial q} \int\int_{-\infty}^{\infty} g(\tilde{y}(q) + v\tilde{\beta} + w\tilde{e}^\perp)\,\mathrm{d}v\frac{\mathrm{d}w}{w}\Big|_{q=s} \end{aligned}$$

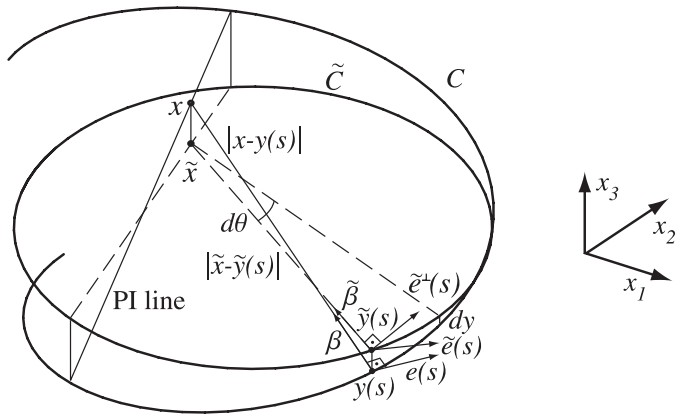

Figure 2. Illustration of the proof of theorem 2.

$$= \frac{1}{\sqrt{\beta_1^2+\beta_2^2}} \frac{\partial}{\partial q} \int_{-\infty}^{\infty} \hat{g}(\tilde{e}^{\perp}, \tilde{y}(q)\cdot\tilde{e}^{\perp} + w)\frac{\mathrm{d}w}{w}\bigg|_{q=s}$$
$$= \frac{\dot{\tilde{y}}(s)\cdot\tilde{e}^{\perp}}{\sqrt{\beta_1^2+\beta_2^2}} \int_{-\infty}^{\infty} \hat{g}'_p(\tilde{e}^{\perp}, p)\frac{\mathrm{d}p}{p - \tilde{x}\cdot\tilde{e}^{\perp}} \tag{12}$$

where $\tilde{x} = (x_1, x_2)$, $\tilde{y} = (y_1, y_2)$, and $\hat{g}$ denotes the 2D Radon transform of g. Since $\tilde{e}^{\perp}$ has no component along the x_3 axis, $\dot{\tilde{y}}(s)\cdot\tilde{e}^{\perp} = \dot{y}(s)\cdot\tilde{e}^{\perp}$. Recall that $\tilde{e}^{\perp}$ is actually a function of s and x. By assumption, x is fixed and can be omitted from the notation. Substituting (12) into (9) we get

$$f(x) = \frac{1}{2\pi^2}\int_{I_{PI}(x)} \frac{\dot{y}(s)\cdot\tilde{e}^{\perp}(s)}{\sqrt{\beta_1^2+\beta_2^2}|x-y(s)|}\int_{-\infty}^{\infty}\hat{g}'_p(\tilde{e}^{\perp}(s), p)\frac{\mathrm{d}p}{\tilde{x}\cdot\tilde{e}^{\perp}(s) - p}\,\mathrm{d}s. \tag{13}$$

As is easily seen

$$\sqrt{\beta_1^2+\beta_2^2}|x-y(s)| = |\tilde{x}-\tilde{y}(s)|. \tag{14}$$

Suppose the origin is at x, and θ denotes the polar angle in the x_1–x_2 plane. Since $\dot{y}(s)\,\mathrm{d}s = \mathrm{d}y(s)$, $(\dot{y}(s)\cdot\tilde{e}^{\perp}(s))\,\mathrm{d}s$ is the projection of the elementary spiral segment $\mathrm{d}y(s)$ onto the direction $\tilde{e}^{\perp}$. By construction, $\tilde{e}^{\perp}$ is perpendicular to $\tilde{\beta}$ and lies in the x_1–x_2 plane. Therefore, dividing by $|\tilde{x}-\tilde{y}(s)|$ gives the increment in the polar angle $\mathrm{d}\theta$ (see figure 2), and the change of variables from s to θ transforms (13) into the standard 2D Radon transform inversion formula:

$$g(\tilde{x}) = \frac{1}{2\pi^2}\int_0^{\pi}\int_{-\infty}^{\infty}\frac{\hat{g}'_p(\tilde{e}^{\perp}(\theta), p)}{\tilde{x}\cdot\tilde{e}^{\perp}(\theta) - p}\,\mathrm{d}p\,\mathrm{d}\theta. \tag{15}$$

Theorem 3. *For $f \in C_0^{\infty}(U)$, (9) transforms into the 2D Radon transform inversion formula in the limit as $h \to 0$.*

Proof. Assume without loss of generality that we want to reconstruct the slice $x_3 = 0$ through f. Represent f as a sum

$$\begin{aligned} f(x_1, x_2, x_3) &= f(x_1, x_2, 0) + f_1(x_1, x_2, x_3) \\ f_1(x_1, x_2, x_3) &:= f(x_1, x_2, x_3) - f(x_1, x_2, 0). \end{aligned} \tag{16}$$

Theorem 2 implies that (9) applied to $f(x_1, x_2, 0)$ is equivalent to the 2D Radon transform inversion formula. Apply now (9) to $f_1(x_1, x_2, x_3)$. The second equation in (16) implies that we can find a smooth function $f_2(x_1, x_2, x_3)$ such that

$$f_1(x_1, x_2, x_3) = f_2(x_1, x_2, x_3)x_3. \tag{17}$$

Since we are interested in reconstructing f_1 only on the plane $x_3 = 0$, $y_3(s) = O(h)$ uniformly in $s \in I_{PI}(x)$ for all such x. By construction we also have $\beta_3(s, x), e_3(s, x) = O(h)$, $s \in I_{PI}(x)$ for all such x. Using (17) write the integral with respect to γ in (9) as follows:

$$\begin{aligned} A(s, x) &= \int\!\!\int_{-\infty}^{\infty} \frac{\partial}{\partial q} f_2(y(q) + v\beta + we)(y_3(q) + v\beta_3 + we_3)\Big|_{q=s} \,\mathrm{d}v \frac{\mathrm{d}w}{w} \\ &= \int\!\!\int_{-\infty}^{\infty} \frac{\dot{y}(s) \cdot \nabla f_2(y(s) + v\beta + we)}{w} \,\mathrm{d}w(y_3(s) + v\beta_3)\,\mathrm{d}v \\ &\quad + \int\!\!\int_{-\infty}^{\infty} \dot{y}(s) \cdot \nabla f_2(y(s) + v\beta + we)\,\mathrm{d}w\, e_3\,\mathrm{d}v \\ &\quad + \int\!\!\int_{-\infty}^{\infty} \frac{f_2(y(s) + v\beta + we)}{w} \,\mathrm{d}w \frac{h}{2\pi}\,\mathrm{d}v. \end{aligned} \tag{18}$$

By construction, $f_2(x_1, x_2, x_3)$ and its derivatives are bounded on compact sets and compactly supported with respect to x_1 and x_2. Therefore, the integrals with respect to v and w in (18) are over compact intervals and $A(s, x) = O(h)$. Integrating $A(s, x)$ with respect to s over $I_{PI}(x)$ with $|I_{PI}(x)| < 2\pi$, we conclude that (9) applied to the difference $f(x_1, x_2, x_3) - f(x_1, x_2, 0)$ produces terms of order $O(h)$, $h \to 0$. □

4. Simplification of the backprojection step of the algorithm

Integrating by parts with respect to s in (9) we obtain an inversion formula in which all the derivatives are performed with respect to the angular variables.

$$\begin{aligned} f(x) = -\frac{1}{2\pi^2} \Bigg\{ &\left[\frac{1}{|x - y(s)|} \int_0^{2\pi} D_f(y(s), \Theta(s, x, \gamma)) \frac{\mathrm{d}\gamma}{\sin\gamma} \right]\Bigg|_{s=s_b(x)}^{s=s_t(x)} \\ &- \int_{I_{PI}(x)} \left(\frac{\partial}{\partial s} \frac{1}{|x - y(s)|} \right) \int_0^{2\pi} D_f(y(s), \Theta(s, x, \gamma)) \frac{\mathrm{d}\gamma}{\sin\gamma}\,\mathrm{d}s \\ &- \int_{I_{PI}(x)} \frac{\beta_s'(s, x) \cdot u(s, x)}{|x - y(s)|} \int_0^{2\pi} (\nabla_{u(s,x)} D_f)(y(s), \Theta(s, x, \gamma)) \cot(\gamma)\,\mathrm{d}\gamma\,\mathrm{d}s \\ &- \int_{I_{PI}(x)} \frac{e_s'(s, x) \cdot u(s, x)}{|x - y(s)|} \int_0^{2\pi} (\nabla_{u(s,x)} D_f)(y(s), \Theta(s, x, \gamma))\,\mathrm{d}\gamma\,\mathrm{d}s \\ &- \int_{I_{PI}(x)} \frac{\beta_s'(s, x) \cdot e(s, x)}{|x - y(s)|} \int_0^{2\pi} \left(\frac{\partial}{\partial\gamma} D_f(y(s), \Theta(s, x, \gamma)) \right) \frac{\mathrm{d}\gamma}{\sin\gamma}\,\mathrm{d}s \Bigg\}. \end{aligned} \tag{19}$$

Here $\beta_s' = \partial\beta/\partial s$, $e_s' = \partial e/\partial s$, and $\nabla_u D_f$ denotes the derivative of D_f with respect to the angular variables along the direction u:

$$(\nabla_u D_f)(y(s), \Theta) = \frac{\partial}{\partial t}\, D_f\left(y(s), \sqrt{1 - t^2}\Theta + tu\right)\Big|_{t=0} \qquad \Theta \in u^{\perp}. \tag{20}$$

For the convenience of the reader a derivation of (19) is presented in appendix B.

As was mentioned in Katsevich (2001a), inversion formulae (9) and (19) are of the FBP type. This means that processing of every cone-beam projection consists of two steps. First, shift-invariant and x-independent filtering along a family of tilted lines on the detector is

performed. Secondly, the result is backprojected to update the image matrix. The most time-consuming portion of any typical three-dimensional FBP algorithm is backprojection. This means that x-dependence of the integrals with respect to γ in (19) and of the coefficients in front of them should be simplified as much as possible.

Let s be fixed. Equation (8) and an easy argument based on the properties of a PI segment (see Katsevich (2001a)) imply that all points $x \in U$ that satisfy $s \in I_{PI}(x)$ and $\beta(s, x) = \beta$ for some $\beta \in S^2$ share the same value $s_2 = s_2(s, x)$. Consequently, they share the same vectors $e(s, x), u(s, x)$. Thus we can write $e = e(s, \beta), u = u(s, \beta)$, and

$$\Theta(s, \beta, \gamma) = \cos\gamma\beta + \sin\gamma e(s, \beta). \tag{21}$$

Using (21) and (19) define

$$\begin{aligned}
\Psi_1(s, \beta) &= \int_0^{2\pi} D_f(y(s), \Theta(s, \beta, \gamma)) \frac{\mathrm{d}\gamma}{\sin\gamma} \\
\Psi_2(s, \beta) &= \int_0^{2\pi} (\nabla_{u(s,\beta)} D_f)(y(s), \Theta(s, \beta, \gamma)) \cot(\gamma)\, \mathrm{d}\gamma \\
\Psi_3(s, \beta) &= \int_0^{2\pi} (\nabla_{u(s,\beta)} D_f)(y(s), \Theta(s, \beta, \gamma))\, \mathrm{d}\gamma \\
\Psi_4(s, \beta) &= \int_0^{2\pi} \left(\frac{\partial}{\partial\gamma} D_f(y(s), \Theta(s, \beta, \gamma)) \right) \frac{\mathrm{d}\gamma}{\sin\gamma}.
\end{aligned} \tag{22}$$

Some of the coefficients can be simplified in a straightforward manner:

$$\begin{aligned}
&\frac{\partial}{\partial s} \frac{1}{|x - y(s)|} = \left. \frac{\beta \cdot \dot{y}(s)}{|x - y(s)|^2} \right|_{\beta=\beta(s,x)} \qquad \beta'_s(s, x) \cdot u(s, x) = -\left. \frac{u(s, \beta) \cdot \dot{y}(s)}{|x - y(s)|} \right|_{\beta=\beta(s,x)} \\
&\beta'_s(s, x) \cdot e(s, x) = -\left. \frac{e(s, \beta) \cdot \dot{y}(s)}{|x - y(s)|} \right|_{\beta=\beta(s,x)}
\end{aligned} \tag{23}$$

where we have used that $\beta \cdot u(s, \beta) = \beta \cdot e(s, \beta) = 0$. The last remaining coefficient can be transformed as follows:

$$e'_s(s, x) \cdot u(s, x) = -e(s, x) \cdot u'_s(s, x) \tag{24}$$

because $e \cdot u \equiv 0$. Since $u(s, x) = u(s, s_2(s, x))$, we have

$$\frac{\partial u(s, x)}{\partial s} = \frac{\partial u(s, s_2)}{\partial s} + \left. \frac{\partial u(s, s_2)}{\partial s_2} \frac{\partial s_2}{\partial s} \right|_{s_2=s_2(s,x)}. \tag{25}$$

From (7) both derivatives $\partial u(s, s_2)/\partial s$ and $\partial u(s, s_2)/\partial s_2$ at $s_2 = s_2(s, x)$ depend actually only on $\beta(s, x)$. To find $\partial s_2/\partial s$ we use the same approach as in Katsevich (2001a).

Recall that the x-ray source is at $y(s)$. Project stereographically the upper and lower turns of the spiral onto the detector plane. Since the detector array rotates together with the source, the detector plane depends on s and is denoted $DP(s)$. It is assumed that $DP(s)$ is parallel to the axis of the spiral and is tangent to the cylinder $y_1^2 + y_2^2 = R^2$ (cf (1)) at the point opposite to the source. Introduce coordinates in the detector plane as follows. Let the d_1-axis be perpendicular to the axis of the spiral, and the d_2-axis be parallel to it. This gives the following parametric curves:

$$\begin{aligned}
&d_1(s' - s) = 2R \frac{\sin(s' - s)}{1 - \cos(s' - s)} \qquad d_2(s' - s) = \frac{h}{\pi} \frac{s' - s}{1 - \cos(s' - s)} \\
&\Delta \leqslant s' - s \leqslant 2\pi - \Delta \quad \text{or} \quad \Delta - 2\pi \leqslant s' - s \leqslant -\Delta
\end{aligned} \tag{26}$$

where Δ is determined by the radius of support of the patient: $\Delta = 2\cos^{-1}(r/R)$ (cf (2)). The top and bottom curves are denoted Γ_{top} and Γ_{bot}, respectively (see figure 3). Let $\hat{x}$ denote

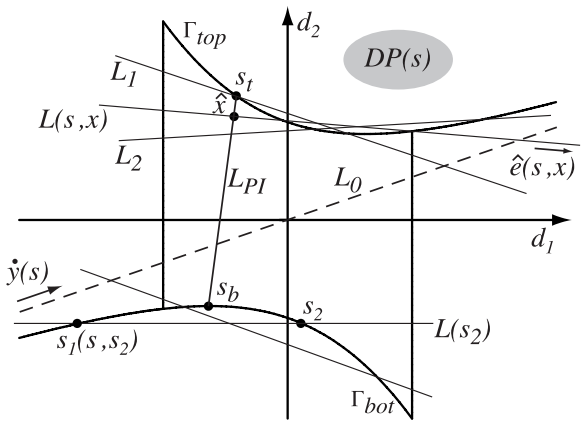

Figure 3. Some of the lines from the family $L(s_2)$ are shown. $L(s, x)$ denotes the line in that family which passes through $\hat{x}$.

the projection of x onto the detector plane. If $s \in I_{PI}(x)$, then $\hat{x}$ is projected into the area between Γ_{top} and Γ_{bot}. Equations (26) imply that the curves Γ_{bot} and Γ_{top} are strictly convex. Also, Γ_{top} approaches L_0 from above as $s' \to s^+$ (in this case $d_1(s' - s) \to +\infty$), Γ_{bot} approaches L_0 from below as $s' \to s^-$ ($d_1(s' - s) \to -\infty$). L_0 denotes the intersection of the plane containing $y(s)$ and parallel to $\dot{y}(s)$, $\ddot{y}(s)$, with the detector plane. L_{PI} denotes the projection of the PI segment onto the detector plane.

Consider a one-parametric family of planes $\Pi(s, s_2)$, $|s_2 - s| < 2\pi$, passing through $y(s)$, $y(s_2)$, and $y(s_1(s, s_2))$. Intersections of these planes with the detector plane $DP(s)$ produces a family of lines $L(s_2)$ (see figure 3). By construction, either $s < s_1 < s_2$, or $s_2 < s_1 < s$, or $s = s_1 = s_2$. Therefore, if $s < s_1 < s_2$, $L(s_2)$ intersects Γ_{top} at two points. If $s_2 < s_1 < s$, $L(s_2)$ intersects Γ_{bot} at two points. And, by continuity, $L(s_2) = L_0$ if $s = s_1 = s_2$.

Suppose $s \in (s_b(x), s_t(x))$, $\hat{x} \neq L_0$, and $s \in I_{PI}(x)$. Instead of solving (8) for s_2, we can find the appropriate line $L(s_2)$ in figure 3 which contains $\hat{x}$. Let $(\hat{x}_1(s), \hat{x}_2(s))$ be the coordinates of $\hat{x}$ on the detector plane $DP(s)$. The equation for s_2 is

$$\frac{\hat{x}_2(s) - d_2(s_2 - s)}{\hat{x}_2(s) - d_2(s_1 - s)} = \frac{\hat{x}_1(s) - d_1(s_2 - s)}{\hat{x}_1(s) - d_1(s_1 - s)} \qquad s_b \leqslant s_2 \leqslant s_t. \tag{27}$$

Obviously, $\hat{x}_{1,2}(s)$ and $d_{1,2}(s_{1,2} - s)$ depend only on $\beta(s, x)$. Consider derivatives of the functions appearing in (27). We have

$$\begin{aligned} \frac{\mathrm{d}}{\mathrm{d}s}\hat{x}_{1,2}(s) &= \nabla_\alpha \hat{x}_{1,2}(\beta)|_{\beta=\beta(s,x)} \cdot \left|\frac{\partial\beta(s,x)}{\partial s}\right| \\ &= \nabla_\alpha \hat{x}_{1,2}(\beta) \cdot \frac{\{|\dot{y}(s)|^2 - [\beta \cdot \dot{y}(s)]^2\}^{1/2}}{|x - y(s)|}\bigg|_{\beta=\beta(s,x)} \end{aligned} \tag{28}$$

where

$$\alpha = \frac{\partial\beta(s,x)}{\partial s} \cdot \left|\frac{\partial\beta(s,x)}{\partial s}\right|^{-1} = -\frac{\dot{y}(s) - [\beta \cdot \dot{y}(s)]\beta}{\{|\dot{y}(s)|^2 - [\beta \cdot \dot{y}(s)]^2\}^{1/2}}\bigg|_{\beta=\beta(s,x)} \tag{29}$$

and ∇_α is defined as in (20). Also, the derivatives $d'_{1,2}(s_2 - s)$, $\partial s_1(s, s_2)/\partial s$, and $\partial s_1(s, s_2)/\partial s_2$ evaluated at $s_2 = s_2(s, \beta)$ depend only on β.

Multiplying (27) out, simplifying, differentiating with respect to s and then solving for $\partial s_2/\partial s$, we conclude that $\partial s_2/\partial s$ is given by a fraction. The numerator of the fraction contains

derivatives of the terms $\hat{x}_{1,2}d_{1,2}$ and $d_{1,2}d_{1,2}$ with respect to s. The denominator of the fraction is

$$\begin{aligned}\kappa := {} & d_1'(s_2-s)(\hat{x}_2(s)-d_2(s_1-s))+d_2'(s_1-s)\frac{\partial s_1(s,s_2)}{s_2}(\hat{x}_1(s)-d_1(s_2-s)) \\ & -d_2'(s_2-s)(\hat{x}_1(s)-d_1(s_1-s))-d_1'(s_1-s)\frac{\partial s_1(s,s_2)}{s_2}(\hat{x}_2(s)-d_2(s_2-s)).\end{aligned} \tag{30}$$

It is shown in Katsevich (2001a) that $\kappa \neq 0$. Also, $\partial s_2/\partial s$ is well defined as $\hat{x} \to L_0$. It is shown in Katsevich (2001a) that in this case $\partial s_2/\partial s \to -1$. Combining this with (28) and (30) implies that we can represent $\partial s_2/\partial s$ in the form

$$\frac{\partial s_2(s,x)}{\partial s} = A(s,\beta)+\frac{B(s,\beta)}{|x-y(s)|}\bigg|_{\beta=\beta(s,x)}. \tag{31}$$

Combining with (24) and (25) and using the argument preceding (21) we get

$$e_s'(s,x)\cdot u(s,x) = v_0(s,\beta)+\frac{v_1(s,\beta)}{|x-y(s)|}\bigg|_{\beta=\beta(s,x)} \tag{32}$$

for some $v_{0,1}(s,\beta)$. Combining (22), (23) and (32) allows us to write inversion formula (19) in the form

$$\begin{aligned}f(x) = -\frac{1}{2\pi^2}\Bigg\{ & \frac{1}{|x-y(s)|}\Psi_1(s,\beta(s,x))\bigg|_{s=s_b(x)}^{s=s_t(x)}-\int_{I_{PI}(x)}\frac{1}{|x-y(s)|}\Phi_1(s,\beta(s,x))\,\mathrm{d}s \\ & -\int_{I_{PI}(x)}\frac{1}{|x-y(s)|^2}\Phi_2(s,\beta(s,x))\,\mathrm{d}s\Bigg\}\end{aligned} \tag{33}$$

where

$$\begin{aligned}\Phi_1(s,\beta) &= v_0(s,\beta)\Psi_3(s,\beta) \\ \Phi_2(s,\beta) &= (\beta\cdot\dot{y}(s))\Psi_1(s,\beta)-(u(s,\beta)\cdot\dot{y}(s))\Psi_2(s,\beta) \\ &\quad +v_1(s,\beta)\Psi_3(s,\beta)-(e(s,\beta)\cdot\dot{y}(s))\Psi_4(s,\beta).\end{aligned} \tag{34}$$

Equation (33) implies that in order to achieve exact reconstruction, the processed projections corresponding to the interior of the PI interval $I_{PI}(x)$ should be backprojected using both the inverse distance squared law and the inverse distance law. Writing the interior terms as follows

$$\frac{1}{|x-y(s)|}\left(\Phi_1(s,\beta(s,x))+\frac{1}{|x-y(s)|}\Phi_2(s,\beta(s,x))\right) \tag{35}$$

we see that for each pair $y(s)$ and x the only two time-consuming quantities that need to be computed are $\beta(s,x)$ and $1/|x-y(s)|$.

Numerical implementation of (33)–(35) can follow the same lines as in Katsevich (2001a, 2001b, 2002b). First, one finds the necessary derivatives of the cone-beam data D_f. Secondly, one computes the functions Ψ_1, Ψ_2, and Ψ_4 by filtering, and Ψ_3 by simple integration. Thirdly, one multiplies Ψ_1 to Ψ_4 by the appropriate weights and combines them into the two functions Φ_1 and Φ_2 according to (34). Finally, Φ_1 and Φ_2 are backprojected into the x-space to update the image matrix according to (33), and the contribution from the endpoints of $I_{PI}(x)$ is added when the current s value is close to either $s_b(x)$ or $s_t(x)$. The fact that the integrals with respect to γ in the definitions of Ψ_1, Ψ_2, and Ψ_4 are convolutions is established analogously to Katsevich (2001a, 2001b, 2002b).

5. Discussion

In this paper we have started a more detailed investigation of the properties of the exact inversion formula proposed in Katsevich (2001a). We established that the formula reduces to the well-known two-dimensional Radon transform inversion if $h \to 0$ or if the phantom is constant along the axis of the spiral. It was shown in Katsevich (2001a) that the formula admits two versions: (9) and (19). The first version is very simple and involves only one filtering step. Its disadvantage is that it requires differencing between neighbouring projections. The second version is somewhat more complicated. It requires more filtering and, as was established here, backprojection must be performed with two weights: $1/|x - y(s)|$ and $1/|x - y(s)|^2$. On the other hand, it has the advantage that all cone-beam projections can be processed completely independently of each other. Some preliminary numerical experiments are presented in Katsevich (2001a). More detailed investigation of the numerical performance of the two versions of the formula will be the subject of future work.

Acknowledgments

This paper is based upon the work supported by the National Science Foundation under grant No 0104033. The author thanks Drs Frederick Noo, Sarah Patch and Michael Silver, whose questions at the 2001 meeting on Fully 3D Image Reconstruction in Radiology and Nuclear Medicine (Pacific Grove, CA) prompted writing of this paper.

Appendix A. Sketch of the proof of theorem 1

Let $x \in U$ be fixed. Considering the integral with respect to γ in (9) we find

$$\int_0^{2\pi} \frac{\partial}{\partial q} \int_0^{\infty} f(y(q) + t(\cos\gamma\beta(s,x) + \sin\gamma e(s,x)))\Big|_{q=s} \frac{1}{t\sin\gamma} t\,\mathrm{d}t\,\mathrm{d}\gamma$$
$$= \frac{-|x - y(s)|}{4\pi} \int_{\mathbb{R}^3} \tilde{f}(\xi)(\xi \cdot \dot{y}(s)) e^{-i\xi\cdot y(s)} \delta(\xi \cdot (x - y(s)))\,\mathrm{sgn}(\xi \cdot e(s,x))\,\mathrm{d}\xi. \tag{A.1}$$

It is clear that any plane through x intersects $C_{PI}(x)$ at least at one point, where $C_{PI}(x)$ is the portion of the spiral corresponding to $I_{PI}(x)$. Introduce the following sets:

$$\begin{aligned}
&\Xi_\psi(x) = \{\xi \in \mathbb{R}^3 : \xi = \lambda u(s,x), s \in I_{PI}(x), \lambda \in \mathbb{R}\}\\
&\mathrm{Crit}(x) = \{\xi \in \mathbb{R}^3 \backslash 0 : \Pi(x,\xi) \text{ contains } y(s_b(x)),\ y(s_t(x)) \text{ or}\\
&\qquad\qquad \Pi(x,\xi) \text{ is tangent to } C_{PI}(x)\} \cup \Xi_\psi(x)\\
&\Xi_1(x) = \{\xi \in \mathbb{R}^3 : \xi \notin \mathrm{Crit}(x) \text{ and } \Pi(x,\xi) \cap C_{PI}(x) \text{ contains one point}\}\\
&\Xi_3(x) = \mathbb{R}^3 \backslash \{\Xi_1(x) \cup \mathrm{Crit}(x)\}.
\end{aligned} \tag{A.2}$$

Recall that $u(s,x)$ was defined above theorem 1. By construction, the sets $\mathrm{Crit}(x)$, $\Xi_{1,3}(x)$ are pairwise disjoint, their union is all of $\mathbb{R}^3$, $\mathrm{Crit}(x)$ has Lebesgue measure zero, and $\Xi_{1,3}(x)$ are open.

Substituting (A.1) into (9) and changing the order of integration (which needs to be properly justified because of the distributions in the integrand), we transform the right-hand side of (9) to the following expression

$$\frac{1}{(2\pi)^3} \int_{\mathbb{R}^3} \tilde{f}(\xi) B(x,\xi)\, \mathrm{e}^{-\mathrm{i}\xi\cdot x}\,\mathrm{d}\xi \tag{A.3}$$

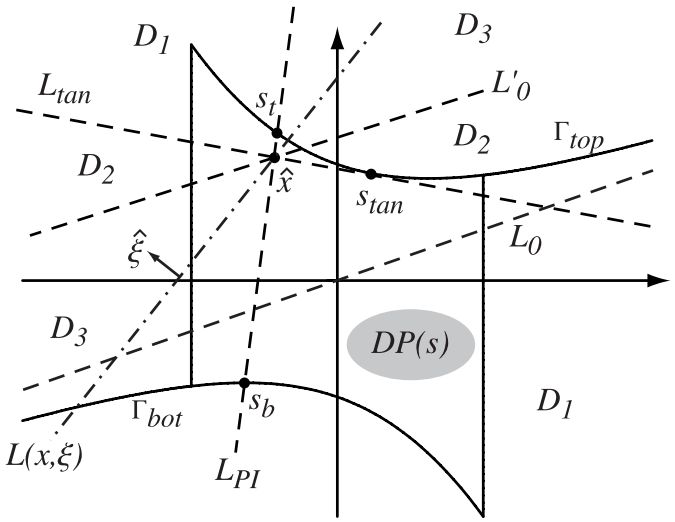

Figure A1. Detector plane shown with various lines through $\hat{x}$.

where

$$B(x,\xi) = \sum_{s_j \in I_{PI}(x)} \operatorname{sgn}(\xi \cdot \dot{y}(s_j)) \operatorname{sgn}(\xi \cdot e(s_j, x)), \xi \in \Xi_1 \cup \Xi_3 \tag{A.4}$$

and $s_j = s_j(\xi, \xi \cdot x)$, $j = 1, 2, \ldots$, denote parameter values corresponding to points of intersection of the plane $\Pi(x,\xi) := \{z \in \mathbb{R}^3 : \xi \cdot (z - x) = 0\}$ with $C_{PI}(x)$. These points are found by solving $\xi \cdot (x - y(s)) = 0$ for s. Since the integral in (A.3) resembles the inverse Fourier transform, we have to prove that the sum in (A.4) equals 1 for $\xi \in \Xi_1 \cup \Xi_3$. Values of $B(x,\xi)$ for $\xi \in \mathrm{Crit}(x)$ are irrelevant, because the set $\mathrm{Crit}(x)$ has measure zero.

Consider various lines through $\hat{x}$ (see figure A1). $L_{\tan}$ denotes the line through $\hat{x}$ and tangent to either Γ_{top} if $\hat{x}$ is above L_0, or Γ_{bot} if $\hat{x}$ is below L_0. In both cases the point of tangency should fall inside the PI parametric interval and, therefore, is unique. The corresponding parameter value will be denoted $s_{\tan}$. If $\hat{x} \in L_0$, by continuity $L_{\tan} = L_0$. L'_0 is the line through $\hat{x}$ and parallel to L_0. Finally, $L(x,\xi)$ is the intersection of $\Pi(x,\xi) \ni y(s)$ with the detector plane. The lines L_{PI}, $L_{\tan}$, and L'_0 split the detector plane into three regions: D_j, $j = 1, 2, 3$. If $\hat{x} \in L_0$, then $L_{\tan} = L_0$ and D_2 collapses into an empty set. If $L(x,\xi) \subset D_1$, $\Pi(x,\xi) \cap C_{PI}(x)$ contains only one point-$y(s)$. If $L(x,\xi) \subset D_2 \cup D_3$, the set $\Pi(x,\xi) \cap C_{PI}(x)$ contains three points of intersection.

In order to evaluate (A.4) we need a simplifying argument. Let $\hat{\xi}$ be a nonzero vector in the detector plane $DP(s)$ perpendicular to $L(x,\xi)$ and pointing into the same half-space as ξ, that is $\xi \cdot \hat{\xi} > 0$ (see figure A1). Fix any nonzero vector $e \in \mathbb{R}^3$ perpendicular to $\beta(s,x)$, and let L be the line in the intersection of $\Pi(x, \beta(s,x) \times e)$ with the detector plane. Analogously, $\hat{e}$ denotes a vector in the detector plane parallel to L and with the property $e \cdot \hat{e} > 0$ (see figure 3 for a vector $\hat{e}(s,x)$, which is obtained by projecting $e(s,x)$ onto $DP(s)$). It turns out that

$$\operatorname{sgn}(\xi \cdot \dot{y}(s)) \operatorname{sgn}(\xi \cdot e(s,x)) = \operatorname{sgn}(\hat{\xi} \cdot \dot{y}(s)) \operatorname{sgn}(\hat{\xi} \cdot \hat{e}(s,x)). \tag{A.5}$$

Thus we can project three-dimensional vectors ξ and $e(s,x)$ onto the detector plane and compute (A.4) using these projections, which is much easier than to deal with the original vectors. Note that $\dot{y}(s)$ is parallel to $DP(s)$.

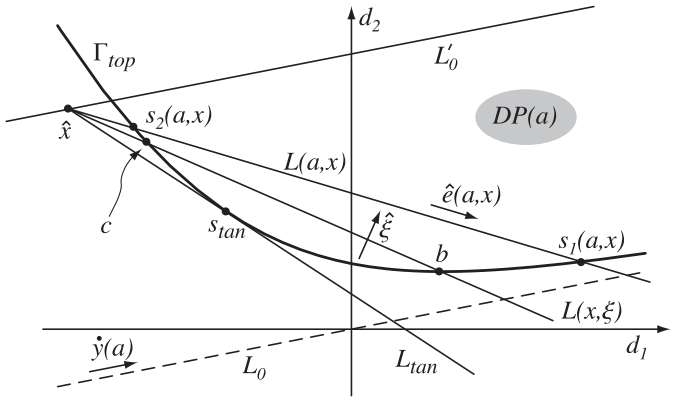

Figure A2. Top half of the detector plane projected from $y(a)$.

If $\xi \in \Xi_1(x)$, there is only one point of intersection. Consequently, $L(x,\xi) \subset D_1$ and it is easily seen from figures 3 and A1 that $\operatorname{sgn}(\hat{\xi} \cdot \hat{e}(s,x)) = \operatorname{sgn}(\hat{\xi} \cdot \dot{y}(s))$. Hence, from (A.4) and (A.5):

$$B(x,\xi) = \operatorname{sgn}(\xi \cdot \dot{y}(s)) \operatorname{sgn}(\xi \cdot e(s,x)) = 1 \qquad \xi \in \Xi_1(x). \tag{A.6}$$

If $\xi \in \Xi_3(x)$, the intersection contains three points: $y(a)$, $y(b)$, and $y(c)$, $a < b < c$. Suppose first that the focal point is located at $y(b)$. By observing that the other two points of intersection are located below and above $y(b)$ we conclude that on the plane $DP(b)$ one has $L(x,\xi) \in D_3$. Again, from figures 3 and A1 and formula (A.5) we see that the contribution of the middle point to the sum in (A.4) equals 1.

The contributions of the top and bottom points $y(a)$ and $y(c)$ are a little harder to evaluate: each one can be either 1 or -1. Consider the detector plane $DP(a)$, where a is the smallest value of the parameter among the three points. Since $y(a)$ is the lowest point of intersection and there are two more points in $\Pi(x,\xi) \cap C_{PI}(x)$, the line $L(x,\xi)$ intersects the part of Γ_{top} corresponding to $a < s < s_t(x)$ at two points (see figure A2). Two cases are possible (recall, $\xi \notin \operatorname{Crit}(x)$):

Case 1. If $c < s_2(a,x)$, then $L(x,\xi)$ passes between $L(a,x)$ and $L_{\tan}$. This case is illustrated by figure A2. Consequently,

$$\operatorname{sgn}(\hat{\xi} \cdot \dot{y}(a)) = \operatorname{sgn}(\hat{\xi} \cdot \hat{e}(a,x)) \qquad \operatorname{sgn}(\xi \cdot \dot{y}(a)) \operatorname{sgn}(\xi \cdot e(a,x)) = 1. \tag{A.7}$$

Case 2. If $c > s_2(a,x)$, then $L(x,\xi)$ passes between $L(a,x)$ and L_0', so

$$\operatorname{sgn}(\hat{\xi} \cdot \dot{y}(a)) = -\operatorname{sgn}(\hat{\xi} \cdot \hat{e}(a,x)) \qquad \operatorname{sgn}(\xi \cdot \dot{y}(a)) \operatorname{sgn}(\xi \cdot e(a,x)) = -1. \tag{A.8}$$

Consider now the detector plane $DP(c)$. Since $y(c)$ is the highest point of intersection and there are two more points in $\Pi(x,\xi) \cap C_{PI}(x)$, $L(x,\xi)$ intersects the part of Γ_{bot} corresponding to $s_b(x) < s < c$ at two points.

Suppose the triple $\{a,b,c\}$ is such that case 1 occurs. This implies that $L(x,\xi)$ in the $DP(c)$-plane is between $L(c,x)$ and L_0' as shown in figure A3. Indeed, otherwise we get (see figure A4):

$$s_2' < a < b < s_1' = \psi(c - s_2') + s_2' \qquad s_2' := s_2(c). \tag{A.9}$$

Case 1 occurs if

$$s_1 = a + \psi(s_2 - a) < b < c < s_2 \qquad s_2 := s_2(a). \tag{A.10}$$

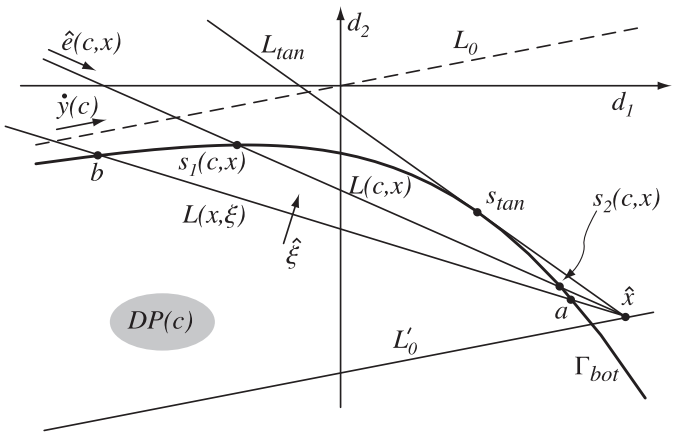

Figure A3. Correct location of the line $L(x, \xi)$, which is compatible with case 1. The bottom half of the detector plane is shown.

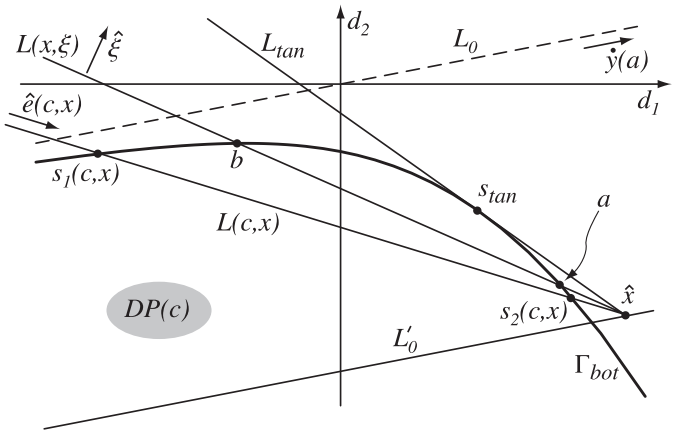

Figure A4. The arrangement of lines shown here is incompatible with case 1. The bottom half of the detector plane is shown.

From (A.9), (A.10)

$$a + \psi(s_2 - a) < \psi(c - s_2') + s_2' \qquad s_2' < a < c < s_2. \tag{A.11}$$

Since $0 < \psi' < 1$,

$$a + \psi(s_2 - a) > s_2' + \psi(s_2 - s_2') > s_2' + \psi(c - s_2') \tag{A.12}$$

and this contradicts (A.11). Therefore,

$$\operatorname{sgn}(\hat{\xi} \cdot \dot{y}(c)) = -\operatorname{sgn}(\hat{\xi} \cdot \hat{e}(c, x)) \qquad \operatorname{sgn}(\xi \cdot \dot{y}(c)) \operatorname{sgn}(\xi \cdot e(c, x)) = -1. \tag{A.13}$$

If the triple $\{a, b, c\}$ is such that case 2 occurs, we obtain analogously that the image of $L(x, \xi)$ in the $DP(c)$-plane is between $L(c, x)$ and $L_{\tan}$ and

$$\operatorname{sgn}(\hat{\xi} \cdot \dot{y}(c)) = \operatorname{sgn}(\hat{\xi} \cdot \hat{e}(c, x)) \qquad \operatorname{sgn}(\xi \cdot \dot{y}(c)) \operatorname{sgn}(\xi \cdot e(c, x)) = 1. \tag{A.14}$$

Let us now summarize. If $\xi \in \Xi_1(x)$, $B(x, \xi) = 1$ from (A.6). If $\xi \in \Xi_3(x)$, there are three points of intersection: $s_b(x) < a < b < c < s_t(x)$. The contribution of the middle point $y(b)$ to the sum in (A.4) equals 1, and the contributions of the points $y(a)$, $y(c)$ cancel each other (see (A.7) and (A.13), (A.8) and (A.14)). So in all cases the value of the sum equals 1.

Appendix B. Derivation of formula (19)

Substituting the identity

$$\frac{\partial}{\partial q} D_f(y(q), \Theta(s,x,\gamma))|_{q=s} = \frac{\partial}{\partial s} D_f(y(s), \Theta(s,x,\gamma)) - \frac{\partial}{\partial q} D_f(y(s), \Theta(q,x,\gamma))|_{q=s} \tag{B.1}$$

into (9) and integrating the first term by parts with respect to s we immediately get the first two lines in (19). Consider now the second term on the right in (B.1). For simplicity, we will drop all the arguments of Θ from the notation. Since $|\Theta| \equiv 1$, $\Theta \cdot \Theta'_s \equiv 0$, and $\Theta \perp u$, then

$$\Theta'_s = [\Theta'_s \cdot (\Theta \times u)](\Theta \times u) + [\Theta'_s \cdot u]u \tag{B.2}$$

and

$$\frac{\partial}{\partial q} D_f(y(s), \Theta(q,x,\gamma))|_{q=s} = [\Theta'_s \cdot (\Theta \times u)]\nabla_{\Theta \times u} D_f + [\Theta'_s \cdot u]\nabla_u D_f \tag{B.3}$$

where $\nabla_\alpha D_f$ is defined as in (20). Using that $\Theta = \cos\gamma\beta + \sin\gamma e$, the second term on the right in (B.3) produces the third and the fourth integrals in (19). Finally, in view of the relations

$$\begin{aligned} \Theta \times u &= (\cos\gamma\beta + \sin\gamma e) \times u = -\sin\gamma\beta + \cos\gamma e = \Theta'_\gamma \\ \Theta'_s \cdot (\Theta \times u) &= (\beta'_s \cdot e)\cos^2\gamma - (\beta \cdot e'_s)\sin^2\gamma = \beta'_s \cdot e \end{aligned} \tag{B.4}$$

we conclude that the first term on the right in (B.3) produces the last integral in (19). Here we have used that $\beta \cdot e \equiv 0$ and, hence, $\beta \cdot e'_s = -\beta'_s \cdot e$. Additionally, using the first equation in (B.4) and (20) (which applies because $\Theta'_\gamma \perp \Theta$),

$$\nabla_{\Theta \times u} D_f(y(s), \Theta(s,x,\gamma)) = \nabla_{\Theta'_\gamma} D_f(y(s), \Theta(s,x,\gamma)) = \frac{\partial}{\partial \gamma} D_f(y(s), \Theta(s,x,\gamma)). \tag{B.5}$$

References

Bruder H *et al* 2000 Single slice rebinning reconstruction in spiral cone-beam computed tomography *IEEE Trans. Med. Imaging* **19** 873–87

Danielsson P E *et al* 1997 Towards exact reconstruction for helical cone-beam scanning of long objects. A new detector arrangement and a new completeness condition *Proc. 1997 Meeting on Fully 3D Image Reconstruction in Radiology and Nuclear Medicine (Pittsburgh, 1997)* ed D W Townsend and P E Kinahan, pp 141–4

Defrise M, Noo F and Kudo H 2000 A solution to the long-object problem in helical cone-beam tomography *Phys. Med. Biol.* **45** 623–43

Grangeat P 1991 Mathematical framework of cone beam 3D reconstruction via the first derivative of the Radon transform *Mathematical Methods in Tomography* (*Lecture Notes in Mathematics vol 1497*) ed G T Herman, A K Louis and F Natterer (Berlin: Springer) pp 66–97

Grangeat P 2001 Fully three-dimensional image reconstruction in radiology and nuclear medicine *Encyclopedia of Computer Science and Technology* vol 44, ed A Kent and J G William (New York: Dekker) pp 167–201

Katsevich A 2001a Improved exact FBP algorithm for spiral CT *Adv. Appl. Math.* submitted

Katsevich A 2001b An inversion algorithm for spiral CT *Proc. 2001 Int. Conf. on Sampling Theory and Applications (May 13–17, 2001, University of Central Florida)* ed A I Zayed, pp 261–5

Katsevich A 2002a Microlocal analysis of an FBP algorithm for truncated spiral cone beam data *J. Fourier Anal. Appl.* at press

Katsevich A 2002b Theoretically exact FBP-type inversion algorithm for spiral CT *SIAM J. Appl. Math.* at press

Kudo H, Noo F and Defrise M 1998 Cone-beam filtered-backprojection algorithm for truncated helical data *Phys. Med. Biol.* **43** 2885–909

Kudo H and Saito T 1997 An extended cone-beam reconstruction using Radon transform *1996 IEEE Med. Imaging Conf. Record (IEEE 1997)* pp 1693–7

Kachelriess M, Schaller S and Kalender W A 2000 Advanced single-slice rebinning in cone-beam spiral CT *Med. Phys.* **27** 754–72

Natterer F 1994 Recent developments in x-ray tomography *Lect. Appl. Math.* **30** pp 177–98

Noo F, Kudo H and Defrise M 1998 Approximate short-scan filtered-backprojection for helical CB reconstruction *Conf. Record 1998 IEEE Nuclear Science Symposium (Toronto, Ontario Canada)* vol 3 (Piscataway, NJ: IEEE) pp 2073–7

Ramm A G and Zaslavsky A I 1992 Inversion of incomplete cone-beam data *Appl. Math. Lett.* **5** 91–4

Schaller S *et al* 2000 Exact Radon rebinning algorithm for the long object problem in helical cone-beam CT *IEEE Trans. Med. Imaging* **19** 361–75

Tam K C 1995 Method and apparatus for converting cone beam x-ray projection data to planar integral and reconstructing a three-dimensional computerized tomography (CT) image of an object *US Patent* 5257183

Tam K C 1997 Cone-beam imaging of a section of a long object with a short detector *Information Processing in Medical Imaging (Lecture Notes in Computer Science, vol 1230)* ed J S Duncan and G R Gindi (Berlin: Springer) pp 525–30

Turbell H and Danielsson P-E 2000 Helical cone beam tomography *Int. J. Imaging Syst. Technol.* **11** 91–100